Characterization and Modeling of Flying Ballast Phenomena in High-speed Train Lines

Benigno J. Lazaro, Ezequiel Gonzalez
Universidad Politecnica de Madrid
28040 Madrid, Spain

Manuel Rodriguez
SENER
28760 Tres Cantos, Spain

Miguel Rodriguez, Salvador Osma, Jorge Iglesias
ADIF
28003 Madrid, Spain

Abstract

A full scale experimental investigation of the flying ballast phenomena taking place in high-speed train lines is presented. The aerodynamic load associated to the flow induced by the train passage has been characterized by Pitot-static and hot-film anemometry. Using the available Pitot-static data, each hot-film sensor undergoes an individual calibration for every flow realization. Ensemble averaged information of the mean and fluctuating air velocities at different height from the ballast bed is obtained as a function of the relative train passage time. The transport of ballast particles is characterized using high-speed video recording of particles positioned in selected locations of the track.

The aerodynamic measurements indicate that most of the time the turbulent flow developing close to the ballast bed approximately follows a turbulent Couette structure that can be characterized by a friction velocity and a temporally modulated equivalent sand roughness, with the air velocity exhibiting strong fluctuating activity down to the surface layer located over the ballast bed. The flow structure is completed with strong perturbation events triggered by the passage of the rolling stock lower wall topology details. The high-speed video recording data allows to construct preliminary statistics of the motion of ballast particles. The aerodynamic measurements are used as input to simple models intended to describe some aspects of the ballast transport. The obtained preliminary results indicate that some scaling laws and transport trends can be captured by the proposed, simplified description.

Introduction

One of the aspects limiting the operating velocity of high-speed trains is the so-called ballast projection phenomena [1]. It describes the ability that the train passage has to set in motion and lift solid particles resting over the track. For tracks lay down over a ballast bed, the ballast particles provide elements to fuel the process. Eventually, the particles can hit the rolling stock lower wall, creating safety and maintenance problems, and hampering the passenger comfort. The high-speed train operators require limiting the occurrence of ballast projection, prompting research efforts to understand its nature [1-7].

The mechanisms involved in the phenomena are complex. The actions setting in motion the ballast particles are caused by the train motion. In particular, the aerodynamic field caused by the rolling stock entrainment is known to play a key role [1-3]. Under proper conditions, this field is able to set in motion some ballast particles. In order for that to occur, the aerodynamic load must counteract gravity and the reactions exerted by the ballast bed over the specific particle. For the high Reynolds numbers involved in the problem, the aerodynamic load over the particles scale with the square of the train velocity. As a result, the ballast projection requires a threshold train velocity, after which the probability of occurrence increases as the train velocity does. The train operation speed is then limited if the number of ballast projection events is to be controlled. The evolution of a ballast particle set in motion by the aerodynamic load also depends on the actions exerted over it by the ballast bed. These

occur when the particle collides with one or several stationary ballast particles and with the surface of the sleepers.

Resulting from the turbulent flow character and from the ballast bed geometry, both the aerodynamic load and the inter-particle actions are stochastic processes that can be characterized by their statistic structure. An adequate modelling of both is essential to correctly describe the projection statistics. The high-speed train operation requires the ballast impact to be a very rare event, making its prediction particularly difficult.

In order to model the flying ballast phenomena it is necessary to gain understanding in the description of the flow structure developing close to the ballast bed. In addition a correct description of the inter-particle actions is also necessary [4]. In this work full scale measurements aimed at characterizing the turbulent flow created by the rolling stock motion is presented. Both mean and fluctuation velocities are investigated. In addition high speed video recording of the motion of ballast particles is used to construct basic statistical information that can help in checking aspects of the modelling effort.

Experimental set-up

The experimental characterization of the flying ballast phenomena discussed in this work was entirely achieved by performing full scale, field measurement campaigns in a commercial high-speed track. The field campaigns were directed to achieve two well defined objectives. The first one pursued the characterization of the aerodynamic field developing over the ballast surface following the passage of a high-speed train. In addition, work was performed to obtain quantitative information on the transport of ballast particles.

The test site for all the measurements was located in the Madrid-Barcelona high-speed line operated by ADIF (figure 1). Measurements stations were prepared in the two tracks that compose the line. The stations were lay down in a straight sector of the line comprising the transition from an embankment to a trench. The embankment is 20 m high and develops over a length of 120 m. The trench has a maximum elevation of 6 m and is characterized by 45º slopes. The measurements were performed using both commercial traffic and through specific, dedicated tests. The sleepers have their longitudinal axis with a 0.6 m separation. The ballast particles have a mean density of 2700 Kg/m^3, with a volume/area mean size of 45 mm. The horizontal plane tangent to the particles is nominally placed 233 mm below the top of rail (TOR) plane, whereas the base of the sleepers is located 203 mm below the TOR plane at the track's plane of symmetry (figure 2).

Figure 1: General view of the test site.

The characterization of the aerodynamic field developing over the ballast bed was achieved through the combined use of Pitot-static and hot-film anemometry probes. To describe the orientation and location of the probes, a coordinate system attached to them will be used, having its x axis aligned with the track axis and oriented along the direction of motion, while the y axis is aligned in the vertical direction and oriented upwards (figure 2). The origin of the coordinate system is placed in the plane of symmetry of the track and in the mid plane of a reference sleeper, with the x axis being included in the TOR plane.

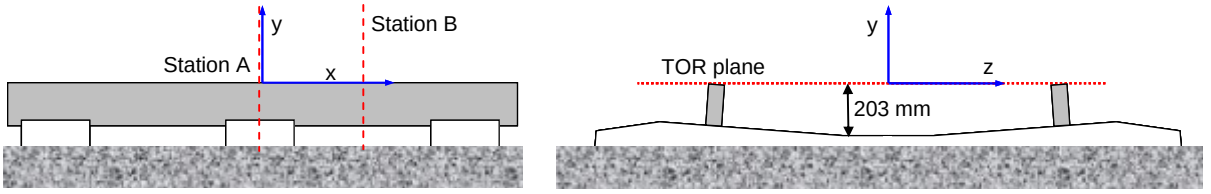

Figure 2: Coordinate system used in the experimental characterizations. Left: view through a plane containing the track axis. Right: view through a vertical plane perpendicular to the track axis.

The sensing areas of the different Pitot-static and hot-film anemometry probes were arranged in x=constant planes. In order to determine possible differences in the aerodynamic field developing along the track, two different measurement stations were characterized. Station A (x=0) is positioned in the reference sleeper's mid plane, whereas station B (x=0.3 m) is located in the mid-plane separating two consecutive sleepers (figure 2). The nominal location of the probes in the y-z plane is displayed in figure 3. All the probes have their axis aligned with the mean flow direction x. The Pitot-static pressure ports are installed in the z=32 mm vertical plane, whereas the hot-film probes are positioned along the z=-32 mm vertical plane. A total of 5 Pitot-static probes are used in the characterizations, placed at vertical distances of y=-3, -48, -93, -138, and -183 mm. In this fashion, the probe closer to ground is placed at a height of 20 mm from the top of sleeper plane and at 50 mm from the horizontal plane tangent to the ballast bed. For each hot-film there is a Pitot-static probe located at the same height and at equal distance with respect to the track's symmetry plane (z=0).

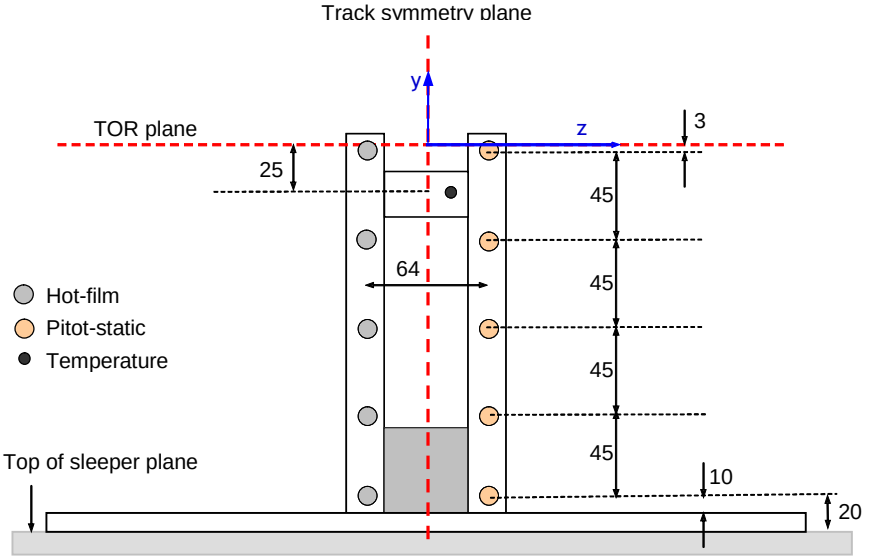

Figure 3: Schematic view of the position assigned to the different probes used in the aerodynamic field characterization. Plane x=constant viewed looking along the +x direction.

Each Pitot-static probe was constructed around a 110 mm long, 5 mm diameter tube (figure 4). The Pitot hole was located at the tube upstream end, in a 5 mm recessed, flat head configuration intended to minimize alignment errors in the total pressure measurement. The static pressure probe consisted of 4 holes, 2 mm diameter, located 50 mm downstream from the tube upstream end . The measurement ports were connected to 1 mm inner diameter pneumatic lines, 300 mm long. At the end of the lines, installed in a supporting beam, there was a transducer unit (Pressure Systems ESP-32HD) that included a set of 32 piezo-resistive differential pressure sensors with a ±2.5 KPa measurement range and an analogue to digital conversion able to provide digital outputs with a 500 Hz quasi-simultaneous conversion rate. The temporal response of the pneumatic system was estimated to have a 240 Hz fundamental eigen-frequency. The differential pressures were taken with respect to a reference pressure port maintained at a constant level during the passage of the train. Thus, each sensor could provide, with respect to this pressure level, the static and total pressure, as well as velocity magnitude measurements. No provisions were made to filter the transducer output since only ensemble averaged measurements were considered with these probes.

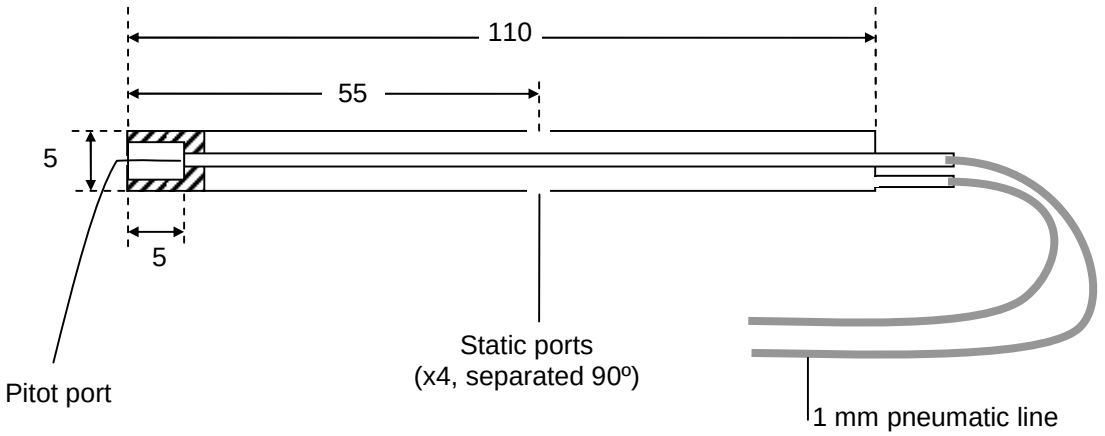

Figure 4: Pitot-static probe scheme.

The hot-film probes were one-dimensional sensors from Dantec Dynamics (55R01), mounted in 4 mm diameter supports. In order to minimize the risk of probe damage with rain, all the sensors were mounted with their sensible films placed in a vertical plane. Therefore, they were sensitive to velocities in the x-z plane. The hot-film signals were connected to signal processors through 20 m long, BNC cables. The hot-film frequency response was 20 KHz, which permitted obtaining measurements of the turbulent activity characterizing the train passage. Figure 5 shows the set of Pitot-static and hot film probes installed in their supporting beam. The aerodynamic characterization probes were completed with a piezo-resistive transducer to measure the absolute pressure level and a Pt-100 temperature sensor installed in between the Pitot-static and hot-film rakes (figure 3).

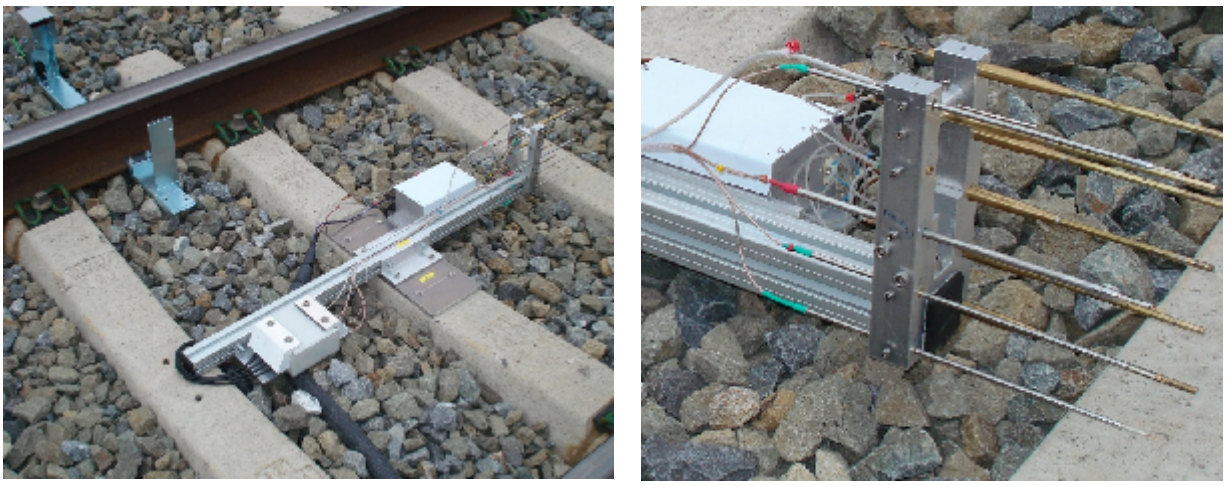

Figure 5: Installed Pitot-static and hot-film rakes. Left: general view showing also the infrared train position sensor. Right: detailed view of the probes.

The position of the train was determined using an infrared light gate sensor that produced a 0 to 10 V output swing when its light path was blocked. The axis of the light path was set 5 cm above the TOR plane in order to capture the passage of the wheels' axes. The characteristic rising time of the light gate was 1 ms, giving a 0.1 m uncertainty in the determination of the train position. An additional light gate sensor, placed 300 m upstream of the measurement location, provided a train passage trigger signal. The different signals processors and computers were installed in a environment controlled, rain-proof cabinet that allowed a continuous, automatic operation of the complete measurement system (figure 1).

Each Pitot-static probe was individually calibrated against a traceable 2-channel LDV anemometry in a blow-down, open return wind tunnel. Under one-dimensional flow, the transfer function was characterized by a ±1% accuracy in the mean velocity. A novel, in-situ calibration procedure for the hot-film data was used to determine the mean and turbulent velocity associated to each train

passage. The calibration procedure used the velocity decay observed after the passage of each individual train. The decay law at a particular y location was obtained from the Pitot-static probe and served to determine the hot-film calibration constants according to a modified King's law [8]:

$$V_{eff} = \left(\frac{e_{hf}^2 - A}{B} \right)^n \qquad (1)$$

In expression (1) e_{hf} represents the output voltage from the hot-film, V_{eff} is the effective velocity measured by the hot-film and A, B, and n are the calibration constants. The wind tunnel facility used to calibrate the Pitot-static probes was also the vehicle to determine the accuracy of the in-situ calibration procedure. For that purpose, the wind tunnel was given a ramp-up, stabilization, and ramp-off command sequence. The in-situ hot-film calibration against the Pitot-static probe was performed using the ramp-off portion of the sequence. Figure 6 gives the comparison between the velocities obtained from the Pitot-static probe and the in-situ calibrated hot-film, in a calibration experiment where the approaching flow is turbulent with turbulence intensity levels similar to those found in the field characterizations. The two data sets exhibit mean velocity differences below ±2% in the [10,45] m/s velocity range, in spite that the Pitot-static data shown in figure 6 displays some statistical fluctuations associated to its relatively low sampling rate.

In specific train passages, cubic test particles of size similar to the mean ballast particle size and different densities were placed over a reference sleeper. The high-speed camera was then used to register the particle evolution.

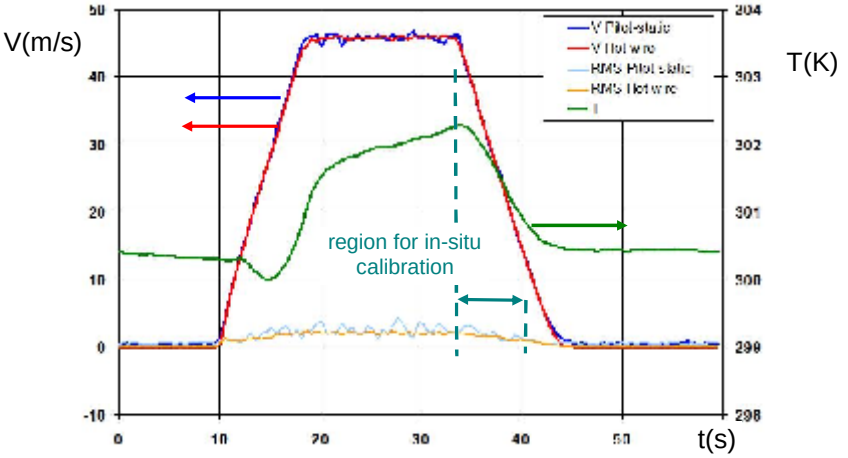

Figure 6: Results of the hot-film in-situ calibration procedure. Comparison of velocities obtained with the Pitot-static and hot-film probes in a ramp-up, stabilization and ramp-off wind tunnel sequence. Approaching flow temperature evolution also shown.

In addition, the transport of ballast particles was characterized by placing marked particles of different sizes in specific locations over one sleeper. Recording their position after the passage of the train allowed to obtain the displacement of the marked particles.

Analysis of experimental results

Hereafter all the data will be presented in non-dimensional form. The train velocity U_T , the nominal rolling stock-top of sleeper plane vertical distance H, and the air density ρ will be the magnitudes selected to obtain the non-dimensional data. The data will be presented based on a specific high speed train type. The rolling stock-track nominal vertical distance will be obtained in regions located sufficiently away both from the interface plane separating consecutive cars and from any auxiliary equipment installed on the rolling stock under floor. With this choice the non-dimensional mean ballast particle size is $O(10^{-1})$. Table 1 shows the non-dimensional position of the different sensors used in the aerodynamic characterization. The vertical coordinate of the ballast bed wall y_{WB} is taken as half the mean ballast size below the vertical coordinate of the horizontal plane tangent to the ballast bed.

Item	y
Nominal ballast bed wall (y_{BW})	-0.670
Top of sleeper plane	-0.530
Rake sensor 1	-0.480
Rake sensor 2	-0.360
Rake sensor 3	-0.245
Rake sensor 4	-0.125
Rake sensor 5	0.010
Top of rail plane	0.000
Nominal rolling stock lower wall	0.470

Table 1: Non-dimensional vertical coordinates of relevant reference locations.

The aerodynamic field has been characterized performing ensemble averages over a number of train passages, where the data is classified according to the value of the non-dimensional time measured with respect to a reference instant of arrival (phased measurements). The latter can be computed from the signal provided by the train position light gate. Selecting t=0 as this instant, phased mean and standard deviation values of a non-dimensional fluid magnitude φ can be defined as:

$$\Phi = \frac{\sum_{k=1}^{N}\left[\sum_{i=1}^{M(k)}\varphi(i,k)\psi(i,k,t)\right]}{\sum_{k=1}^{N}\left[\sum_{i=1}^{M(k)}\psi(i,k,t)\right]}, \quad \sigma_{\varphi}(t) = \left\{\frac{\sum_{k=1}^{N}\left[\sum_{i=1}^{M(k)}\left(\varphi(i,k)\psi(i,k,t)-\bar{\varphi}(t)\right)^2\right]}{\sum_{k=1}^{N}\left[\sum_{i=1}^{M(k)}\psi(i,k,t)\right]-1}\right\}^{1/2} \tag{2}$$

In expressions (2) φ(i,k) represents the value of φ measured at the discrete sampling instant t_i, within the k train passage, whereas N represents the total number of passages and M(k) is the total number of φ samples recorded in the k passage. The phase function ψ(i,k,t) is defined as:

$$\psi(i,k,t) = \begin{cases} 1 & (t-\Delta t/2) < t(i,k) < (t+\Delta t/2) \\ 0 & \text{otherwise} \end{cases} \tag{3}$$

The interval size Δt must be selected large enough to have enough number of samples in a given phase time t, and small enough as to be able to detect changes associated to the passage of the rolling stock's topology details. Typically this requires Δt=O(1). For the data presented here a Δt=2.5 interval was selected.

The flow configuration within the trackbed-rolling stock inter-space exhibits some elements that resemble a turbulent Couette configuration, where the lower wall incorporates roughness elements given by the ballast and sleeper configuration. The upper wall topology is, however, more complex, as it includes the details of the rolling stock lower wall. For a characteristic train speed of 300 Km/h, the Reynolds number based on the trackbed/rolling stock velocity difference and the characteristic height H is over 10^6, whereas the characteristic Reynolds number based on the friction velocity and ballast particle size is $O(10^3)$, indicating that the ballast bed acts as a fully rough wall. Under these conditions, and for heights from the ballast bed larger than the characteristic ballast particle size, the instantaneous flow velocity is mainly one-dimensional:

$$u = \bar{u} + u' \tag{4.1}$$
$$v = v' \tag{4.2}$$
$$w = w' \tag{4.3}$$

where $\bar{u} = O(1)$, and u', v, w'<<1. With this scaling, the instantaneous velocity measured both by the Pitot-static and hot-film probes becomes:

$$v_{eff-Pitot} = \sqrt{u^2+v^2+w^2} \approx \bar{u} + u' \tag{5.1}$$
$$v_{eff-hotfilm} = \sqrt{u^2+v^2+w^2} \approx \bar{u} + u' \tag{5.2}$$

Therefore, the instantaneous velocity measured by the anemometry probes is approximately the longitudinal velocity component. Figure 7 shows the Pitot-static and hot-film phase averaged velocity measured at sensor position 1 (y=-0.480). This height corresponds to a distance over the top of sleeper plane similar 1/2 of the mean ballast particle size. Thus, the registered flow can be taken as indicative of the flow that would be experienced by a particle placed over the sleeper. Both mean and standard deviation obtained through expressions (2) are shown for a single composition train. The average process has been performed over 400 train passages, giving a 95% confidence statistical error associated to each individual phase lower than 1.5%. The hot-film and Pitot-static mean velocities exhibit differences smaller than ±5% in all the train passage interval, thus validating the in-situ hot-film calibration procedure. The temporal evolution of the velocity standard deviation shows very similar behavior for both probes, with the Pitot-static data giving levels 7% higher than the ones obtained from the hot-film probe. The hot-film data should give the correct fluctuation level, since the Pitot-static fluctuations are affected by the pneumatic line and differential pressure transducer transfer functions. The pneumatic line transfer function will typically have a low-pass filter character with second order subcritical behavior at specific eigen-frequencies. Therefore, depending on the fluctuating velocity spectral contents, the standard deviation of the velocity computed from the Pitot-static data can be higher or lower than the hot-film given value. It should be noticed however that the differences in the fluctuation value given by the two techniques are small, particularly if the Pitot-static data is adjusted by introducing an O(1) correcting coefficient.

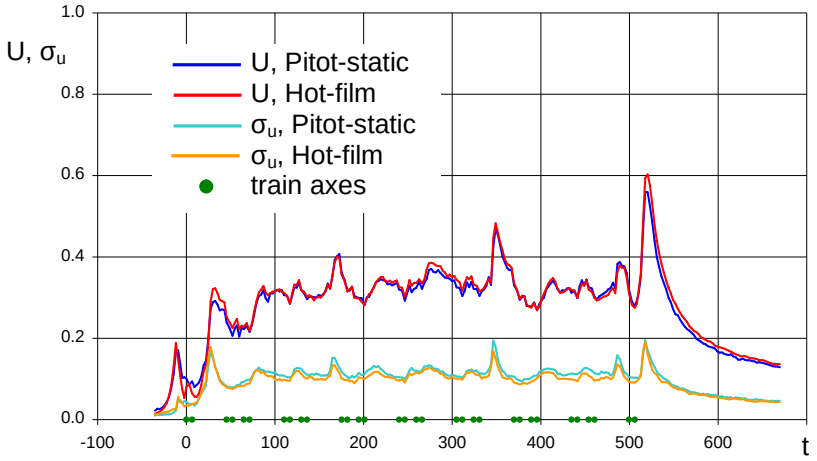

Figure 7: Temporal evolution of the phase-averaged velocity registered at sensor position 1 (y=-0.48) by the Pitot-static and hot-film probes. Station A (over the sleeper). Phase averaged mean and standard deviation of both probes are shown, together with the position of the train axes.

The composition of the train includes 8 cars arranged in a 1+6+1 configuration where the first and the last are head cars. As a result, the rolling stock lower wall topology has a symmetry plane located at the middle of the train length. The phase averaged mean velocity profile presented in figure 7 follows this configuration. As the train passes through the sensor position, the entrainment flow stars to built up progressively. At t~100, approximately corresponding to 1/5 of the train length or the end of the second car, the entrainment flow has been established at this low vertical position. The characteristic mean flow velocity over the sleeper is 1/3 of the train velocity, whereas the rms level of the longitudinal velocity fluctuations is 1/10 of the train velocity. The phase averaged mean velocity exhibits features associated to the passage of the rolling stock lower wall topology. Thus, at the interface plane between two consecutive cars there is a small local decrease in the measured mean velocity. At times t=170 and 350 there is a region of substantially increased mean and rms velocity level connected to the presence of auxiliary equipment in the rolling stock lower wall, symmetrically placed with respect to the train mid length plane. The registered velocity signature linked to the two topology details is not the same, as most likely the equipment is not symmetric with respect to its vertical mid plane. Two additional strong perturbations can be detected in the head cars located at the train's front and rear end. The velocity signature linked to the train downstream end is particularly significant, as the topology of the rolling stock lower wall creates a large area restriction that promotes the mean velocity to reach peak values close to 60% of the train velocity at ground level.

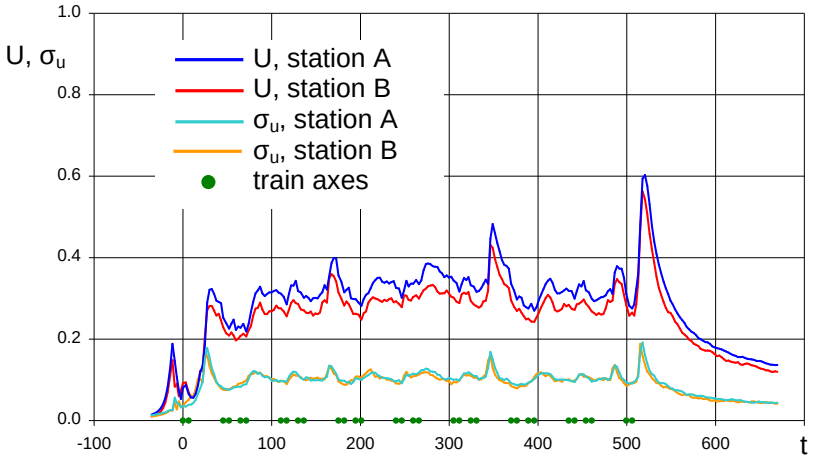

Figure 8: Comparison between the temporal evolution of the phase averaged longitudinal velocity registered by sensor position 1 (y=-0.48) at station A (over the sleeper) and B (between sleepers). Mean and standard deviation for both stations are shown, together with the position of the train axes.

A comparison of the longitudinal phased averaged velocity measured at stations A (over sleeper) and B (between sleepers), at y=-0.48, close above the ballast bed, is given in figure 8. The temporal evolution of the phased averaged mean velocity in both stations follow a similar pattern, with the velocities at station A showing 15% higher levels than those registered at station B. This difference is connected to the blockage to the train entrainment flow introduced by the sleeper. On the other hand the longitudinal velocity fluctuations display similar non-dimensional levels in both stations, indicating that the turbulent structure linked to the trackbed/rolling stock entrainment flow dominates over the fluctuations introduced by the sleeper's local topology.

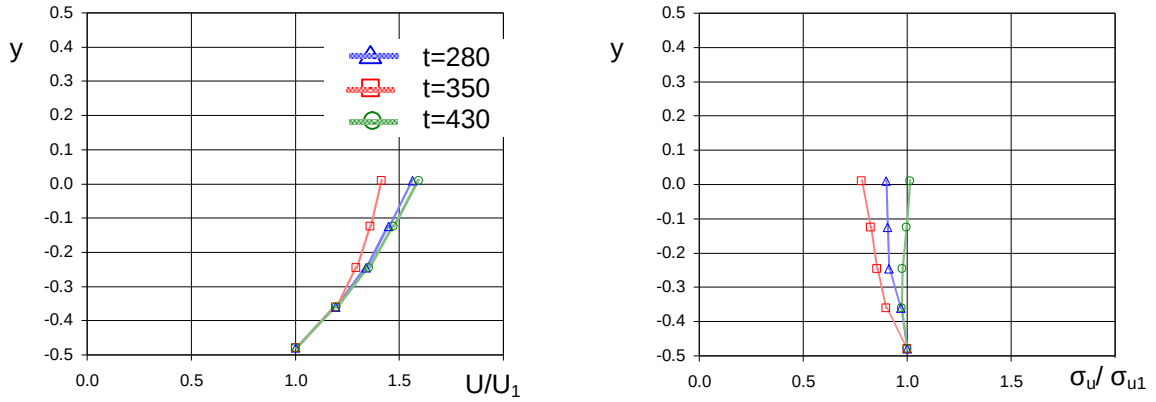

Figure 9: Vertical profiles of the phase averaged velocity obtained at station B (between sleepers) and different instants of the train passage. Left: mean velocity. Right: rms velocity. Data scaled with values obtained at y=-048.

Phased averaged, vertical velocity profiles obtained for different instants of the train passage are shown in figure 9. The different data have been referred to the values achieved at the lower sensor vertical location (y=-0.48). Instant t=280 corresponds to the passage of a mid section of car # 5, whereas t=350 occurs during the passage of car #6 and coincides with the moment where the lower sensor velocity exhibits a peak value linked to the auxiliary equipment installed in the rolling stock under floor. Finally, t=430 corresponds to the instant just before the passage of the car #7 rear axis.

Excluding the data corresponding to the peak perturbation, the phase averaged velocity profiles obtained at t=280 and 430 exhibit a fair degree of collapse when referred to the data obtained at y=-0.48. This seems to indicate that, away from the instants when the large scale details of the rolling stock under floor pass by, the mean velocity profile in the region adjacent to the trackbed is rather similar, with small modulations in its phase averaged values. Furthermore, for these instants, the velocity fluctuations display an approximately uniform profile across the vertical coordinate. This is what would be expected in a turbulent Couette flow, suggesting the connection between this flow and

the turbulent structure developing adjacent to the trackbed over a significant portion of the train passage, away from regions where the strong perturbations induced by the rolling stock underfloor topology are propagated to the trackbed region.

At the time where the peak perturbation in the phase averaged velocity is registered (t=350), there is a significant deviation of the profiles with respect to the pattern just described. In addition, the velocity fluctuations significantly deviate from a uniform profile. These characteristics can be understood considering the convection of the underfloor induced perturbation by the train movement and taking into account that, in a reference frame linked to the train, the perturbation is not aligned in the vertical direction, but trails backwards as the trackbed is approached.

We will assume that, away from the time intervals where the strong perturbations pass by, the flow structure developing close to the ballast bed incorporates a logarithmic layer. This feature characterizes high Reynolds numbers wall flows including turbulent boundary layers and Couette flows, and appear when the distance to the wall and the friction velocities are the only relevant scales. In that case it is possible to estimate the friction velocity u_f from the measured mean velocity profiles:

$$u_f = k\frac{(U_l - U_m)}{\ln((y_l - y_{BW})/(y_m - y_{BW}))} \tag{6}$$

In expression (6) the sub indices l,m refer to rake sensor positions l and m, y_{BW} is the vertical coordinate of the ballast bed wall, and k=0.41 is the Von Karman constant. An alternative route to compute the friction velocity is to consider the solution of the Reynolds stress tensor in the logarithmic layer of a turbulent Couette flow with fully rough walls [9]:

$$\overline{u'_i u'_j} = u_f^2\begin{bmatrix} 2.78 & -1 & 0 \\ -1 & 1.39 & 0 \\ 0 & 0 & 1.39 \end{bmatrix}, \Rightarrow u_f = \sqrt{\frac{\overline{u'^2}}{2.78}} = 0.36\cdot\sigma_u \tag{7}$$

Table 2 compares the non-dimensional friction velocity obtained from the experimental data presented in figure 9 using expressions (6) and (7). In expression (6), and in order to minimize experimental errors, it has been selected y_l=-0.125 and y_m=-0.360, whereas the longitudinal fluctuation to be used in expression (7) is taken as the average value in those vertical locations.

t	u_f, expression (6)	u_f, expression (7)
280	0.061	0.061
430	0.057	0.058

Table 2: Friction velocity estimated according to expressions (6) and (7).

The two estimates produce very similar values, suggesting both the validity of the log layer flow structure and the experimental data coherence. Introducing the fully rough wall hypothesis and knowing the friction velocity allows to estimate the flow equivalent sand roughness r_s:

$$r_s = (y - y_{BW})\cdot\exp\left(k\left(8 - \frac{U}{u_f}\right)\right) \tag{8}$$

The application of expression (8) to the data presented in figure 9 gives an equivalent sand roughness of 0.62 at t=280 and 0.74 at t=430. In both cases r_s=O(1), whereas the ballast particle size is O(10^{-1}), indicating that the turbulent flow is controlled by the details of the rolling stock under floor topology.

Ballast transport modelling

The motion of individual ballast particles occurs as a result of the forces and torques induced on them by the passage of the train. As the train passes by, the actions induced on a single ballast particle include the aerodynamic load created by the entrainment flow and the contact forces transmitted by

the ballast bed. In addition, the particle is subject to gravity. In this framework, the equations governing the motion of a single particle are the conservation of linear and angular momentum:

$$\rho_B d_B^3 \frac{d\vec{v}_B}{dt} = -\rho_B d_B^3 \vec{g} + \vec{F}_a + \vec{F}_c \tag{9.1}$$

$$\rho_B d_B^5 \dot{I}_B \cdot \frac{d\vec{\omega}_B}{dt} - \rho_B d_B^5 \left(I_B \times \vec{\omega}_B\right) \cdot \vec{\omega}_B = \vec{M}_a + \vec{M}_c \tag{9.2}$$

In these equations the sub index B refers to the ballast particle, whereas (F_a, M_a) and (F_c, M_c) denote, respectively, the forces and torques linked to the aerodynamic load (sub index a) and to the contact actions from the track (sub index c). The angular momentum equation is solved in a coordinate system attached to the particle, whit ω_B, I_B representing, respectively, its angular velocity and inertia tensor.

For typical velocities of current high-speed train operations the motions of ballast particles are rare events. The high speed video recordings suggest identifying different stages in the process:

1. Induction: The perturbation induced by the train passage act over the particle, who acquires an initial linear and angular speed.
2. Ballast surface transport: characterized by the particle center of mass being at distances from the nominal ballast bed of the order of the particle size. In this stage the particle is accelerated in the x direction by the aerodynamic load while suffering frequent contact actions from the ballast bed.
3. Particle fly: characterized by the particle acquiring a positive vertical speed large enough to promote a time interval where the particle is free from contact actions. The positive vertical speed is typically imparted by the contact actions when the particle reaches enough kinetic energy. Depending on the initial vertical velocity, the particle fly can end in an impact over the rolling stock under floor or in an impact against the ballast bed. After it, the ballast particle can repeat stages 2 and 3.

Modelling of both the aerodynamic and contact terms is complex. In the linear momentum equation, expressions can be proposed for the aerodynamic and the combined gravity-contact forces terms:

$$\vec{F}_a = \frac{1}{2}\rho d_B^2 |\vec{v}|\vec{v} \tag{10.1}$$

$$-\rho_B d_B^3 \vec{g} + F_c = -\rho_B d_B^3 \vec{g} H(y) + \rho_B d_B^3 |\vec{v}_B| \delta(t - t_{ci}) \vec{c}_{ci} \tag{10.2}$$

Expression (10.1) implies that the particle/train velocity ratio is very small and that the entrainment flow is quasi one-directional. In expression (10.2) H(y) represents the Heavyside function, $\delta(t\text{-}t_{ci})$ is the Dirac delta function associated to impact time t_{ci} and c_i denotes a non-dimensional vector that describes the effect of the "i" particle-ballast bed impact. Incorporating these expressions, equation (9.1) can be casted in non-dimensional form:

$$\frac{du_B}{dt} = \tilde{\rho} u^2 + |\vec{v}_B| \delta(t - t_{ci}) c_{ix} \tag{11.1}$$

$$\frac{dv_B}{dt} = -\tilde{g} H(y) + |\vec{v}_B| \delta(t - t_{ci}) c_{iy} \tag{11.2}$$

The non-dimensional parameters appearing in equations (11.1) and (11.2) are:

$$\tilde{\rho} = \frac{c_D}{2} \frac{\rho}{\rho_B} \frac{H}{d_B}, \quad \tilde{g} = \frac{gH}{U_T^2} \tag{12}$$

In order to integrate equations (11.1) and (11.2) the velocity u, and the coefficients c_{ix}, c_{iy} must be modelled following an statistical approach. For u, the relevant information can be extracted from the characterization of the aerodynamic field presented in the previous section. We will assume that the velocity field created by the passage of a train of length L near the ballast bed can be specified through the friction velocity u_f. and the train passage non-dimensional time L/H. The statistical

representation of the impact coefficients c_{ix}, c_{iy} can be specified by defining their probability density function. Assuming that this information is known, non-dimensional analysis can be used to write the functional dependence of the average position reached by a particle that is initially released at location (x_{B0}, y_{B0}) with zero velocity:

$$\langle x_B \rangle = F_x\left(t, \tilde{\rho}, \tilde{g}, \mathrm{pdf}\left(c_{ix}, c_{iy}\right), L/H, u_f, x_{B0}, y_{B0}\right) \quad (13.1)$$

$$\langle y_B \rangle = F_y\left(t, \tilde{\rho}, \tilde{g}, \mathrm{pdf}\left(c_{ix}, c_{iy}\right), L/H, u_f, x_{B0}, y_{B0}\right) \quad (13.2)$$

The probability of impact over the rolling stock under floor P_I is given by the population of particles that reach the condition $y_B \sim 0.5$. Therefore we can write:

$$P_I = P_I\left(\tilde{\rho}, \tilde{g}, \mathrm{pdf}\left(c_{ix}, c_{iy}\right), L/H, u_f, x_{B0}, y_{B0}\right) \quad (14)$$

Under specific conditions, equations (11.1) and (11.2) can readily provide useful information. Let us assume that the particle is initially released over the top of sleeper plane and that at the end of the induction process the particle leaves the sleeper surface with a very small velocity. In that case, the equations of motion of the ballast particle until it hits the ballast bed can be written as:

$$\frac{du_B}{dt} = \tilde{\rho} u_f^2 f\left(x_{B,} y_B, t\right); \quad \frac{dx_B}{dt} = u_B \quad (15.1)$$

$$\frac{dv_B}{dt} = -\tilde{g}; \quad \frac{dy_B}{dt} = v_B \quad (15.2)$$

$$x_B(0) = 0,\ y_B(0) = y_{B0}; \quad u_B(0) = v_B(0) = 0 \quad (15.3)$$

If the ensemble average of $f(x_B,y_B,t)$ is independent of the particle position and time, the ensemble averaged longitudinal position achieved at the end of the particle flight, when the vertical particle position is $\langle y_B \rangle = 0$, becomes:

$$\langle x_{BF} \rangle = \frac{\tilde{\rho}}{\tilde{g}} u_f^2 \langle f \rangle = \frac{c_D}{2}\left(\frac{\rho}{\rho_B}\right)\left(\frac{H}{d_B}\right)\frac{U_T^2}{gH}\left(u_f^2 \langle f \rangle\right) \quad (16))$$

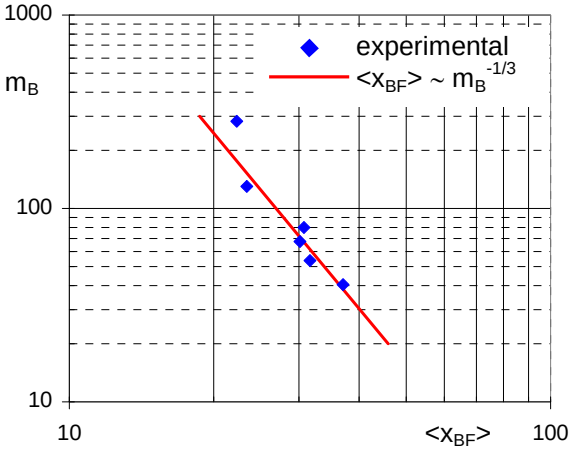

Figure 10: Average longitudinal distance $\langle x_{BF} \rangle$ travelled by ballast particles of mass m_B initially located over the sleeper.

Expression (16) indicates the dependence of the longitudinal particle displacement with different parameters, including the ballast particle material and size (ρ_B,d_B) , and the train velocity and design (U_T,H,u_f,f). For a given ballast density, train type and velocity, the distance transported scales as the inverse of the particle size, i.e., proportional to $m_B^{-1/3}$ with m_B being the mass of the ballast particle. Figure 10 gives the average longitudinal distance travelled by ballast particles initially placed over the sleeper measured from the high speed video recordings, after the passage of a train type with given velocity, suggesting the validity of the above mentioned scaling.

Conclusions

The characteristics of the aerodynamic field developing in the rolling stock-track inter-space of high speed trains have been experimentally investigated. Pitot-static probes and hot-film sensors have been used to obtain the air velocity field developing on the passage of a high speed train. A novel in-situ calibration procedure has been applied to obtain the hot-film calibration curve for each individual sensor and train passage. Two different measurement stations have been characterized: one over a reference sleeper and other located between two consecutive sleepers. The ensemble averaged anemometry data phased to the position of the train over the measurement station reveal that, close to the ballast bed, the mean velocity achieves values close to 1/3 of the train velocity, whereas the standard deviation of the velocity fluctuations are of the order of 1/10 of the train velocity. Similar temporal velocity evolutions are found at both measurement stations, with slightly higher velocities developing over the sleeper as a result of the imposed local flow blockage. The ensemble averages are temporally modulated by the influence of the details in the rolling stock under floor topology, including the presence of axes, interfaces between cars, and auxiliary equipment. Away from the regions greatly perturbed by the rolling stock under floor topology, the flow structure close to the ballast bed is found to have a rather universal structure when the velocity profiles are referred to the values achieved over the ballast bed. In addition the vertical profile of the velocity fluctuations is approximately uniform. These findings suggest that the flow region close to the trackbed resembles a logarithmic layer flow established over a fully rough wall, characterized by a friction velocity close to 0.06 of the train velocity and an equivalent sand roughness that depends on the train's relative position, scaling with the details of its lower wall topology.

High speed video recording of the ballast particles motion help clarifying some of the mechanisms involved in their transport. The process includes an induction stage where the particle is set in motion, followed by a longitudinal transport stage close to the ballast bed that is propelled by aerodynamic forces, and where the solid/solid contact actions play a central role. When the particle has reached sufficient longitudinal momentum, the contact actions can lead to the particle gathering enough vertical momentum to initiate a fly ballistic trajectory (ballast projection). Simple models can be lay down to detect the key controlling non-dimensional parameters. The application of the models to simple transport scenarios suggest their validity to obtain scaling trends.

Acknowledgements

Support received from the Spanish Ministry of Science and Innovation through project Aurigidas and from the European Commission through project Aerotrain is greatly acknowledged.

References

[1] Quinn, A.; Hayward, M.; Baker, C.; Schmid, F;, Priest, J; Powrie, W. A full-scale experimental and modelling study of ballast flight under high-speed trains. Proc. IMechE Part F: J. Rail and Rapid Transit. Vol. 224, 2 (2010).

[2] Ido, A.; Saitou, S.; Nakade, K.; Ikura, S. Study on under-floor flow to reduce ballast flying phenomena. Proc. World Congress on Rail Research, Seoul (2008).

[3] Kwon, H.; Park, C. An experimental study on the relationship between ballast flying phenomenon and strong wind under high speed train. Proc. World Congress on Rail Research, Montreal (2006).

[4] Kaltenbach H., Gautier P., Agirre G., Orellano A., Schroeder-Bodenstein K., Testa M.,Tielkes T. Assessment of the aerodynamic loads on the trackbed causing ballast projection: results from the DEUFRAKO project Aerodynamics in Open Air (AOA). Proc. World Congress on Rail Research, Seoul (2008).

[5] Sima M., Gurr A., Orellano A. Validation of CFD for the flow under a train with 1:7 scale wind tunnel measurements. Proc. BBAA VI, Milano (2008).

[6] Deeg P., Jönsson M., Kaltenbach H., Schober M., Weise M. 2008. Cross-comparison of measurement techniques for the determination of train induced aerodynamic loads on the track bed. Proc. BBAA VI, Milano (2008).

[7] Saussine, G.; Masson, E.; Thomas-Jean, J.; Paradot, N.; Allain, E.; Josse, F. Railway ballast flying phenomenon : from numerical computations toward risk assessment. EUROMECH 509: Vehicle Aerodynamics, Berlin (2009).

[8] Bruun, H. Hot-wire Anemometry. Oxford Univ. Press (1995).

[9] P. Libby. Introduction to Turbulence. Taylor and Francis (1996).